frontiers | Frontiers in Earth Science

TYPE Original Research
PUBLISHED 02 February 2023
DOI 10.3389/feart.2023.1100039

OPEN ACCESS

EDITED BY
Maoliang Zhang,
Tianjin University, China

REVIEWED BY
Xiaocheng Zhou,
China Earthquake Administration, China
Yutao Sun,
Hebei GEO University, China

*CORRESPONDENCE
Xiaopeng Liu,
2641996568@qq.com

SPECIALTY SECTION
This article was submitted to Geochemistry, a section of the journal Frontiers in Earth Science

RECEIVED 16 November 2022
ACCEPTED 18 January 2023
PUBLISHED 02 February 2023

CITATION
Li X, Liu X, Zeng X, Wang X, Luo H, Li M, He J and Shi H (2023), Spatial variations of Rn and CO_2 emissions in the Wuzhong–Lingwu region, northwest China.
Front. Earth Sci. 11:1100039.
doi: 10.3389/feart.2023.1100039

Spatial variations of Rn and CO_2 emissions in the Wuzhong–Lingwu region, northwest China

Xinyan Li[1,2], Xiaopeng Liu[1,3]*, Xianwei Zeng[2], Xiaotao Wang[2], Hengzhi Luo[2], Mengya Li[2], Jiawei He[2] and Haikuo Shi[2]

[1]School of Civil and Hydraulic Engineering, Ningxia University, Yinchuan, China, [2]Earthquake Agency of Ningxia Hui Autonomous Region, Yinchuan, China, [3]School of Geography and Planning, Ningxia University, Yinchuan, China

Soil gas Rn and CO_2 in surface rupture and deep-seated fault zones are important indicators for tectonic and seismic activities. The spatial distributions of Rn and CO_2 concentrations and their relationships with earthquakes and stress state in the Wuzhong–Lingwu area of Ningxia, Northwest China, were investigated through field observations based on 76 measurement points, spatial interpolation and six crossing-fault profiles along Yellow River Fault zone (YRF). Observed results of the soil gas Rn and CO_2 in different segments of Yellow River Fault zone illustrated that YRF has features of both strike-slip and certain normal fault characteristics. Moreover, the difference in seismic activity could also account for the differences in gas concentration and relative activity intensity (RAI) in the Yellow River Fault zone. Significant differences in the spatial distributions of Rn and CO_2 were identified in gridded observation mode. By comparing these spatial distributions with the surface latent heat flux (SLHF), volumetric soil water layer (SWVL), and lithology, an anomalous high-Rn area was identified in the east and south Qingtongxia, and associated with Permian sandstone and mudstone in a piedmont setting. Away from a strong impact of irrigation in the Yinchuan Basin, CO_2 anomalies were identified in the transition area between the Yinchuan Basin and the mountains and coincided with a dramatic negative variation of surface latent heat flux, which was considered to reflect humus accumulation, rich organic matter, and strong soil microorganism activity in loosely accumulated mountain alluvial deposits. After excluding gas anomalies related to shallow soils and surface geology, anomalies of Rn and CO_2 in the west of Lingwu were consistent with the distribution of low seismic b-values and frequent seismic activity in plane and profile. According to similar studies in the north-south seismic belts, it is believed that high stress and strong seismic activity increased the permeability of rocks and boosted the gas emission in the west of Lingwu. Base on a crustal thickness variation belt, high-velocity bodies, and in this region, an higher seismic hazard was illustrated. This study offers new insight into combining geochemical characteristics of soil gas and seismological methods to estimate regional seismic hazards.

KEYWORDS

Rn, CO_2, irrigation, b-value, seismic hazards

Introduction

The emission of gases, such as Rn, CO_2, CH_4, and He, from the solid Earth to the near-surface can be increased by tectonic and seismic activity (King et al., 1996; Giammanco et al., 1998; Fu et al., 2005; Al-Hilal and Abdul-Wahed, 2007; Zhou et al., 2010; Fu et al., 2016; Yuce et al., 2017). Previous studies have demonstrated that a difference in stress state can affect the

concentration and type of soil gas, and soil gas surveys have been performed to assess the potential for seismic hazard prediction (Fu et al., 2008; Kumar et al., 2009; Sun et al., 2021). However, along with regional stress state and seismic activity, the concentration of soil gas can also be related to soil types, lithological characteristics, meteorological parameters, crustal thickness and structure, permeable pathways for gas migration, and human activities (Hinkle, 1994; Han et al., 2014; Szabó et al., 2014). Thus, various soil gas sources have been observed around fault zones, among which meteorological sources can be easily distinguished due to their values being significantly lower. Deep crustal/mantle sources usually have higher concentrations than meteorological sources (Yang et al., 2003; Hong et al., 2010; Yuce et al., 2017). However, soil gas compositions in the near-surface were easily contaminated by the environment (Biological activity, agricultural production and industrial pollution, etc.). Therefore, it is necessary to account for anomalies, meteorological factors, and near-surface influences when analyzing the relationship between soil gas variation and seismic activity. Soil gas studies have been conducted in surface fracture zones produced by large earthquakes (Dogan, et al., 2007; Li et al., 2009; Zhou et al., 2010), faults in basins or valleys controlled by structural patterns (Guerra and Lombardi., 2001; Ciotoli et al., 2007; Al-Hilal et al., 2016), deep-seated faults with frequent moderate and strong earthquakes (Weinlich, 2014; Zhou et al., 2017; Sun et al., 2021), and along active faults on a volcanic field (Neri et al., 2011). These studies found that variations in different gas compositions are spatially synchronized, particularly CO_2 and Rn (Guerra and Lombardi., 2001; Ciotoli et al., 2007; Li et al., 2013; Yuce et al., 2017). However, few soil gas studies have been reported in areas affected by human activities, especially agriculture and irrigation; consequently, the sources and distributions of soil gases in agricultural areas remain unclear. Therefore, to prevent possible earthquake hazards and disasters and assess the seismic risk in human activity areas, the primary goals of soil gas investigation were to understand the various factors of soil gas and obtain anomalies boosted by seismic activity.

As a product of uranium (^{238}U) decay, Rn is a natural radioactive idle gas without stable or synthetic isotopes. It is believed that Rn in Earth's substrata continuously escapes from the surface, resulting in detectable surface concentrations (Khilyuk et al., 2000). In addition to its ability to be measured in minute amounts, Rn is relatively non-reactive to other compounds. He, CH_4, H_2, and CO_2 can serve as carrier gases to transport Rn from depth to the surface (Yang et al., 2003). Based on its origin depth and radioactive characteristics, Rn offers the possibility to determine and quantify changes in gas migration duo to tectonic activity. The parent isotope, surface degassing rate, and carrier gas play essential roles in Rn concentration variation. Among the carrier gases, CO_2 is one of the most important. Numerous CO_2 sources have been identified in structurally active zones, including mantle degassing, carbonate metamorphism, and decomposition of organic matter (Irwin and Barnes, 1980); this CO_2 can be transported along deep-seated faults (Baubron et al., 2002). A higher concentration of CO_2 at the surface indicates higher pore pressure in the subsurface, which can contribute to identifying potential seismic zones (Irwin & Barnes., 1980; Ciotoli et al., 2007). However, CO_2 can also offer evidence of shallow sources (Khilyuk et al., 2000), and simultaneous observations of soil gas Rn and CO_2 can facilitate the elimination of interference factors and the identification of deep gas sources.

Ningxia is a sizeable agricultural area located on the upper reaches of the Yellow River; Wuzhong–Lingwu is an important part of the Hetao irrigation area, and is notable for its rice production. The Wuzhong–Lingwu area is also one of the seismically active regions in Ningxia, with moderately strong earthquakes and complex tectonics (Liao et al., 2000; Chai et al., 2001; Ma et al., 2006; Zeng et al., 2021). Owing to the large population and high level of economic development, geophysical observations in this region are significantly affected by human-related factors, making it more challenging to detect effective earthquake precursors. In this study, we measured the spatial distributions of Rn and CO_2 concentrations in soil gas around the main seismogenic faults of the Wuzhong–Lingwu area to identify soil gas anomalies associated with seismic activity and assess regional seismic risk.

Materials and methods

Seismogeological setting

Wuzhong–Lingwu is an arid/semi-arid inland region of northwest China (Figure 1). The south of the region is characterized by folded mountains. The north is the alluvial Yinchuan Basin, formed by the south–north flow of the Yellow River, forming an important agricultural area. The basin is underlain by thick Quaternary sediments. Based on teleseismic P-wave data, the regional crustal thickness is 40–50 km; more specifically, it is 40–49 km in the Wuzhong–Lingwu area (47–49 km in Lingwu; Xu et al., 2018) and 40–43 km in southern Qingtongxia and Guangwu. P-wave tomography indicates a high-velocity anomaly at shallow mid–crustal depths beneath Lingwu town (Zeng et al., 2017). There are eight strike-slip or normal active faults in the study area, including the Yellow River fault (YRF), Niushou Mountain fault (NSMF), Sanguankou fault (SGKF), Luoshan fault (LSF), Chongxing fault (CXF), Xinhuaqiao fault (XHQF), and Yinchuan blind fault (YCBF). The NSMF forms a boundary with Tertiary sediments of the southern Yinchuan graben (Chai et al., 2001). The region experiences moderate to strong seismic activity owing to neotectonic movements; five earthquakes of $M > 5$ have occurred in the Wuzhong–Lingwu area since 1970 (Ma et al., 2006).

Field measurements

According to the distribution of earthquakes and major fault zones, field measurements were taken at 76 sites within 5–10 km of each other in the Wuzhong–Lingwu area during July 2020 (Figure 1). The sample sites are set to gridded observation mode, and the easternmost measuring sites are located along the Yellow River fault, while the westernmost measuring point is located in front of Helan Mountain. Except for sites along fault zones, the site distribution covered the Wuzhong–Lingwu area as evenly as possible. All sample sites shared the same land use type and daily observation period (09:00–17:00 UTC+8) to minimize the influence of meteorology and surface vegetation on soil gas concentrations. To avoid abnormal gas variations caused by significant differences in soil humidity, move the sites when they are located in areas with high humidity area (canals, the Yellow River, freshly irrigated farmland, etc.). The measuring sites should also be located in the thick surface cover layers to facilitate the occurrence of gases. Six profiles were constructed along the YRF in order to explore the relationship

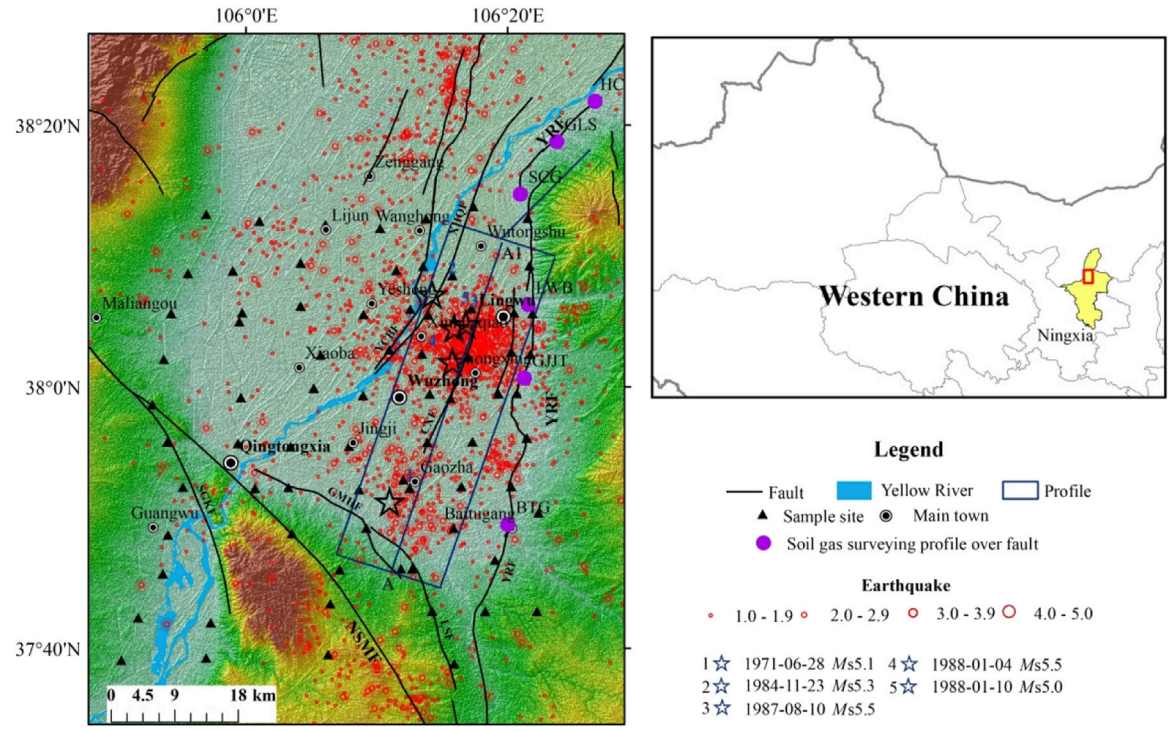

FIGURE 1
Topographical map of the study region showing the main faults, earthquake epicenters, and sampling locations. Abbreviations of the profiles: BTG, Baitugang profile; GJJT, Guojiajiantan profile; LWB, Lingwubei profile; SCG, Shuangchagou profile; GLS, Ganlusi profile; HC, Hengcheng profile. Abbreviations of the faults: YRF, Yellow River fault; NSMF, Niushou Mountain fault; SGKF, Sanguankou fault; LSF, Luoshan fault; CXF, Chongxing fault; XHQF, Xinhuaqiao fault YCBF, Yinchuan blind faul.

between the geochemistry characteristics of soil gas and seismic activity in different segments, including three profiles at the northern segment of Yellow River Fault (YRF_N), two profiles at the middle segment of Yellow River Fault (YRF_M), and one profile at the southern segment of Yellow River Fault (YRF_S). Approximately 14–15 survey points are located on each cross-fault survey line, starting from the center of the fault and extending to both sides (Li et al., 2009). As a starting point, the distance between the two measuring points is 5 m, and it increases successively by 10 m, 15 m, 20 m, 40 m, and 50 m so that the total length of the measuring line is about 240 m–280 m. Soil samples were collected from ~0.8 m depth using a 12-hole hollow steel sampler. Rn concentrations were analyzed using a RAD7 Radon Detector and expressed in Bq/m^3; analytical precision was within 10%, and the detection sensitivity was 9.25 Bq/m^3 operating in the Sniff mode. The Rn concentration for each site was taken as the average of at least three consecutive observations; the error was within ±5%. CO_2 concentrations were measured using an ATG-C60 CO_2 detector (Adtech, China) with a measuring resolution and accuracy of 0.001% and 4%, respectively. The CO_2 concentration for each site was calculated as the average of three measurements; the error was within ±5% under a stable state of continuous measurement.

Data processing

Ordinary kriging (OK) and inverse distance weight (IDW) interpolation were applied to obtain the spatial variation of Rn and CO_2 based on data from the 76 sites. The skewness coefficients of Rn and CO_2 were >0, and kurtosis was >3 (Table 1), indicating that the data did not have a normal distribution. Therefore, logarithmic transformation was performed on the original soil gas data and spatial interpolation was applied to the transformed data, which conformed to a normal distribution. For IDW, we set the inverse distance power value to 2; for OK, a variogram was used to select the spherical function. To assess the accuracy of the spatial interpolation, we used the mean absolute error (MAE; Eq. 1) and root mean square error (RMSE; Eq. 2), which were calculated as follows:

TABLE 1 Statistics of soil gas Rn and CO_2 in gridded observation mode.

CO_2 (%)					Rn (kBq/m^3)				
Max	Min	Ave	Skew	Kurt	Max	Min	Ave	Skew	Kurt
3.95	0.07	0.95	1.69	2.56	36.70	0.07	4.19	3.50	14.94

Max is short for the maximum, and Min is short for the minimum. Skew is short for Skewness, and Kurt is short for Kurtosis.

TABLE 2 CO_2 and Rn concentrations of soil gas at each site in the Wuzhong–Lingwu area.

Site. No	Lon (°E)	Lat (°N)	Date	CO_2 (%)	Rn (kBq/m^3)	Site. No	Lon (°E)	Lat (°N)	Date	CO_2 (%)	Rn (kBq/m^3)
1	106.2295	38.2142	2020/7/14	0.28	3.88	14	106.3412	38.0945	2020/7/15	0.28	0.35
2	106.1706	38.2021	2020/7/14	0.81	1.73	15	105.9491	38.2200	2020/7/16	0.14	6.73
3	106.1010	38.2066	2020/7/14	0.91	2.45	16	105.9258	38.1445	2020/7/16	0.11	2.82
4	106.0171	38.2112	2020/7/14	0.93	1.48	17	105.9045	38.0935	2020/7/16	0.44	9.83
5	105.9831	38.1477	2020/7/14	2.33	7.75	18	105.8951	38.0353	2020/7/16	0.45	3.79
6	106.0693	38.1576	2020/7/14	0.25	0.07	19	105.8807	37.9771	2020/7/16	0.17	2.61
7	106.1914	38.1484	2020/7/14	0.30	0.14	20	106.0864	37.9981	2020/7/16	0.87	3.96
8	106.3650	38.0933	2020/7/15	0.95	0.92	21	105.8995	37.9297	2020/7/16	1.33	12.10
9	106.3308	38.1612	2020/7/15	0.15	0.10	22	105.9897	37.9279	2020/7/16	0.61	1.81
10	106.3612	38.1544	2020/7/15	1.29	2.26	23	106.0565	37.9236	2020/7/16	0.91	24.52
11	106.3588	38.2147	2020/7/15	3.84	4.88	24	106.1313	37.9242	2020/7/16	0.74	3.23
12	106.2895	38.2297	2020/7/15	1.07	2.45	25	106.0950	38.0403	2020/7/17	0.13	0.35
13	106.2628	38.1418	2020/7/15	2.65	5.00	26	105.9935	37.9863	2020/7/17	1.36	1.42
Site. No	Lon (°E)	Lat (°N)	Date	CO_2 (%)	Rn (kBq/m^3)	Site. No	Lon (°E)	Lat (°N)	Date	CO_2 (%)	Rn (kBq/m^3)
27	106.2870	38.0999	2020/7/15	1.42	35.44	41	105.9914	38.0831	2020/7/17	0.35	0.59
28	105.9947	38.0946	2020/7/17	0.29	0.78	42	106.3623	38.0415	2020/7/21	0.43	0.66
29	106.0695	38.1028	2020/7/17	1.67	2.87	43	106.3448	37.9917	2020/7/21	0.90	1.10
30	106.1500	38.0922	2020/7/17	0.52	0.10	44	106.3216	37.9909	2020/7/21	0.27	0.38
31	106.1826	38.0473	2020/7/17	0.65	1.06	45	106.2310	37.9294	2020/7/22	0.23	0.99
32	106.2093	38.0993	2020/7/17	0.31	1.13	46	106.2084	37.8708	2020/7/22	3.18	4.96
33	105.8409	37.6518	2020/7/20	0.36	1.07	47	106.2006	37.8819	2020/7/22	3.26	4.83
34	105.8625	37.7059	2020/7/20	2.40	6.88	48	106.2115	37.7683	2020/7/22	0.70	1.73
35	105.8939	37.7618	2020/7/20	0.62	0.90	49	106.1974	37.7681	2020/7/22	3.91	9.70
36	105.9004	37.8114	2020/7/20	0.73	4.28	50	106.2371	37.7143	2020/7/22	1.01	1.66
37	105.9196	37.8721	2020/7/20	0.91	3.15	51	106.2652	37.6470	2020/7/22	0.16	2.94
38	106.1492	37.9889	2020/7/21	0.81	6.49	52	106.1044	37.6591	2020/7/23	0.13	1.65
39	106.2341	37.9911	2020/7/21	0.62	0.62	53	106.1073	37.7238	2020/7/23	0.10	2.57
40	106.2606	37.9852	2020/7/21	1.04	1.68	54	106.1195	37.7672	2020/7/23	0.54	2.32
Site. No	Lon (°E)	Lat (°N)	Date	CO_2 (%)	Rn (kBq/m^3)	Site. No	Lon (°E)	Lat (°N)	Date	CO_2 (%)	Rn (kBq/m^3)
55	106.2829	38.0380	2020/7/21	0.41	0.28	66	106.1533	37.8202	2020/7/23	0.57	1.19
56	106.3378	38.0451	2020/7/21	1.08	3.66	67	106.1441	37.8693	2020/7/23	0.52	0.14
57	106.0539	37.8720	2020/7/23	2.80	32.50	68	106.2886	37.9302	2020/7/24	1.00	2.57
58	106.0584	37.8130	2020/7/23	0.15	3.51	69	106.3706	37.7138	2020/7/25	0.22	3.08
59	106.0112	37.8708	2020/7/23	1.14	3.64	70	106.3046	37.7139	2020/7/25	0.07	2.57
60	106.2742	37.8730	2020/7/24	1.79	1.53	71	106.3170	37.7793	2020/7/25	0.51	2.71
61	106.2646	37.8201	2020/7/24	1.41	1.73	72	105.9492	37.6545	2020/7/25	1.00	2.40
62	106.3358	37.8290	2020/7/24	0.98	3.30	73	105.9548	37.6994	2020/7/25	1.47	36.70

(Continued on following page)

TABLE 2 (*Continued*) CO_2 and Rn concentrations of soil gas at each site in the Wuzhong–Lingwu area.

Site. No	Lon (°E)	Lat (°N)	Date	CO_2 (%)	Rn (kBq/m^3)	Site. No	Lon (°E)	Lat (°N)	Date	CO_2 (%)	Rn (kBq/m^3)
63	106.3724	37.8395	2020/7/24	0.56	2.59	74	106.2240	38.0422	2020/7/27	0.32	0.14
64	106.3379	37.8728	2020/7/24	0.80	2.01	75	106.2319	38.0917	2020/7/27	0.14	0.10
65	106.3577	37.9346	2020/7/24	1.83	1.61	76	106.2256	38.1536	2020/7/27	2.61	1.45

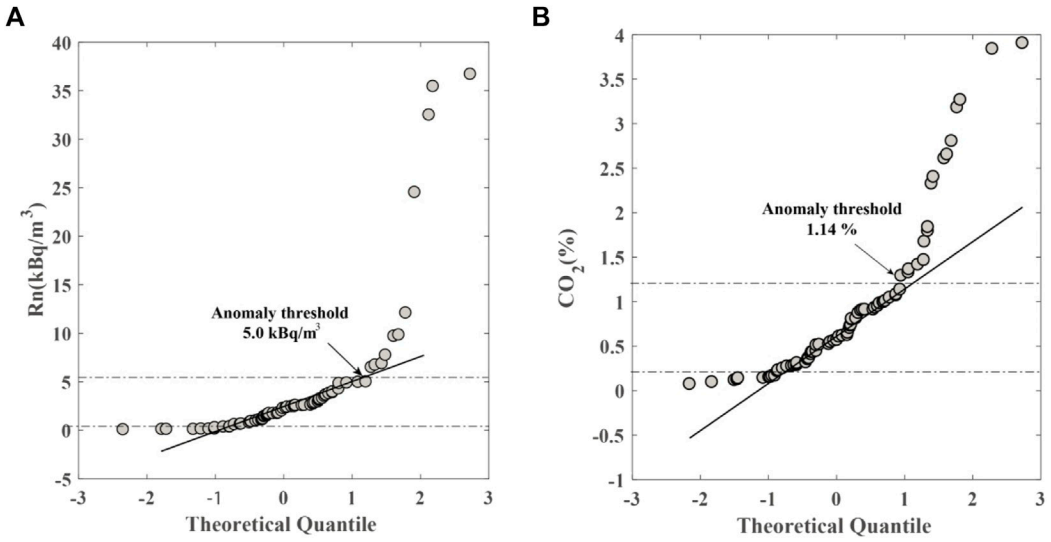

FIGURE 2
Anomaly thresholds of soil gas **(A)** Rn and **(B)** CO_2 estimated by the Q–Q plot method.

TABLE 3 Evaluation of spatial interpolation precision.

Interpolation method	Raster size (km)	Rn	CO_2		
		MAE	RMSE	MAE	RMSE
IDW	1×1	11.46	7.09	0.36	2.55
OK	1×1	98.70	179.53	230.81	424.61

IDW, inverse distance weight interpolation; OK, ordinary kriging; RMSE, root mean square error; MAE, mean absolute error.

$$MAE = \frac{1}{n}\sum_{i=1}^{n}\left|C_{f(i)} - C_{o(i)}\right| \quad (1)$$

$$RMSE = \sqrt{\frac{1}{n}\sum_{i=1}^{n}\left(C_{f(i)} - C_{o(i)}\right)^2} \quad (2)$$

where n is the measured sequence or predicted sequence length, and *Cf(i)* and *Co.(i)* are the measured and predicted values of soil gas, respectively. The method with the smallest error and highest interpolation accuracy was selected to determine the spatial distribution of Rn and CO_2.

Owing to the numerous sources of soil gas, obtaining an anomaly threshold for soil gas is essential for identifying sources related to seismic or tectonic activity. The interquartile range, Z-score, Q–Q plot, and RST methods are widely applied in identifying gas anomalies (Beaubien et al., 2003; Cui et al., 2013; Tramutoli et al., 2013; Jiao et al., 2018). We employed a Q–Q plot to determine the upper and lower limits of the outliers in the Rn and CO_2 data.

The b-value data were obtained from the literature (Zeng et al., 2017; Zeng et al., 2021). Geological records were obtained from the China' Spatial Database of 1:2.5 million digital geological maps. In addition, to examine the influence of surface cover on soil gas concentrations, the monthly data of surface latent heat flux (SLHF; a parameter that reflects heat and moisture exchange between the surface and near-surface atmosphere; Ando and Ueyama, 2017) and volumetric soil water layer (SWVL) data with a spatial resolution of 0.1° × 0.1° were derived from ERA5 land products, they can be download from the Climate Data Store (CDS; https://cds.climate.copernicus.eu); these data were sampled between 09:00 and 17:00 UTC+8. To account for, The background values of SLHF and SWVL were represented by the average value of July from 2016 to 2020 to examine the effect of the hydrothermal characteristics and long-term irrigation processes on soil gas

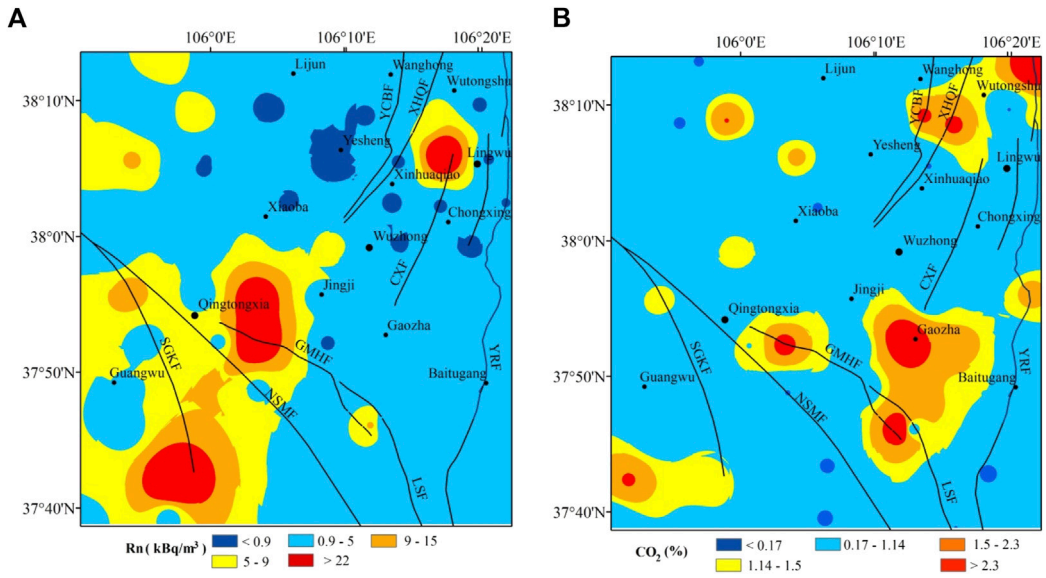

FIGURE 3
Spatial distribution of **(A)** Rn and **(B)** CO_2 concentrations in the Wuzhong–Lingwu area.

TABLE 4 Observed results of the soil gas Rn and CO_2 in the 6 survey profiles in the Yellow River Fault zone.

Profile	Num	Date	Rn (kBq/m³)							CO_2(%)						
			M	M_{max}	M_{min}	Std	A_U	A_L	RAI	M	M_{max}	M_{min}	Std	A_U	A_L	RAI
HC	14	2021.4.14	2.17	5.72	0.27	1.81	3.08	1.27	2.64	0.07	0.16	0.03	0.05	0.10	0.05	2.29
GLS	14	2021.4.20	2.57	4.77	1.12	1.17	3.15	1.98	1.86	0.23	0.43	0.12	0.10	0.28	0.18	1.84
SCG	15	2021.4.19	2.22	5.20	0.81	1.31	2.87	1.56	2.35	0.08	0.15	0.05	0.02	0.09	0.07	1.90
LWB	14	2021.4.26	1.14	1.61	0.48	0.31	1.30	0.99	1.41	0.42	0.67	0.18	0.17	0.51	0.34	1.60
GJJT	14	2021.4.25	2.11	6.96	0.48	2.11	3.17	1.06	3.29	0.49	1.83	0.17	0.48	0.73	0.25	3.74
BTG	14	2021.4.15	1.34	5.72	0.03	1.65	2.16	0.51	4.27	0.67	2.64	0.03	1.04	1.19	0.15	3.93

Num is short for the number of samples, M_{max} is the maximum and M_{min} is s the minimum. Std is short for standard deviation. A_u and A_L, is the upper limit and lower limit of gas anomaly, respectively. RAI, is represent the Relative Activity Intensity. Abbreviations of the profiles: BTG, baitugang profile; GJJT, guojiajiantan profile; LWB, lingwubei profile; SCG, shuangchagou profile; GLS, ganlusi profile; HC, hengcheng profile.

concentration. Equation 3 was used to calculate local spatial variance in SLHF to determine the influence of SLHF on soil gas concentration. (Tramutoli et al., 2005):

$$Diff_r = S_r - S_m \quad (3)$$

where $Diff_r$ is the difference between the SLHF value of the current pixel r (S_r) and its spatial average in a homogenous region (S_m). According to a digital elevation mode; (DEM), the Wuzhong–Lingwu area was divided into mountain and basin regions to calculate local differences.

Following the fault activity determination method used in the past, the mean value M), maximum (M_{max}), minimum (M_{min}), standard deviation (Std) and relative activity intensity (RAI) of soil gas Rn and CO_2 concentration were calculated. Assume the average of each sample site along each line is the background value B), and The upper limit (A_U) and lower limit (A_L) of abnormal Rn and CO_2 concentration in soil gas were calculated by adding 0.5 times standard deviation to the background mean (Yang et al., 2021; Liu et al., 2022). The measured value higher than the upper limit of the anomaly is regarded as the anomaly value related to the fault, and the ratio of the maximum measured value in the anomaly area to the background value is defined as the RAI (Shao et al., 2012):

$$RAI = M_{max}/M \quad (4)$$

Results and discussion

The soil gas Rn and CO_2 results for Wuzhong–Lingwu are shown in Table 2. Rn ranged from 0.07 to 36.7 kBq/m³, with an average value of 4.19 kBq/m³; CO_2 concentration ranged from 0.07% to 3.9%, with an average value of 0.93%. The resultant anomaly threshold values derived using the Q–Q plot method were 5.0 kBq/m³ for Rn and 1.14%

10.3389/feart.2023.1100039

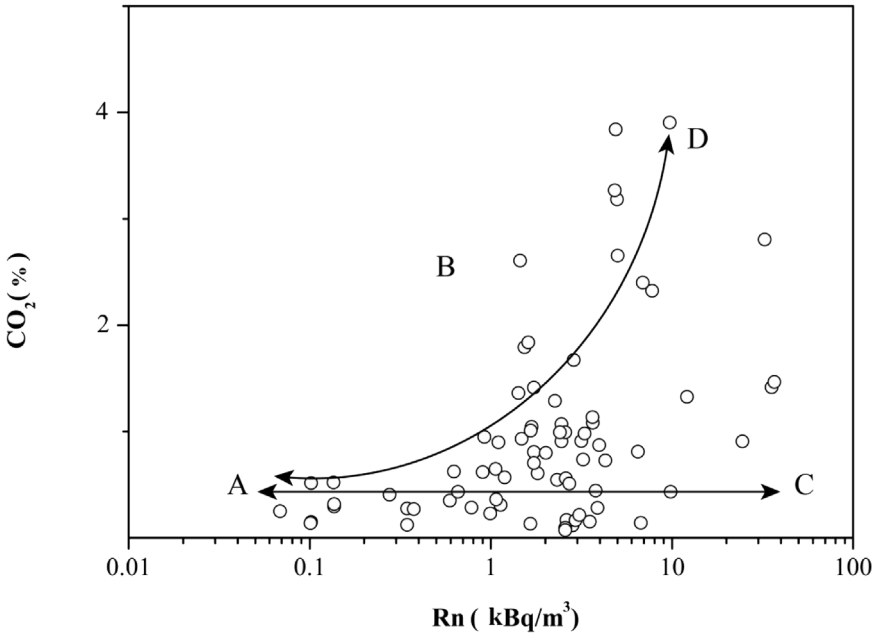

FIGURE 4
Variation diagram of Rn with CO_2 (Part A represents meteorological sources, part C and part B represent shallow sources, Part D represents deep sources).

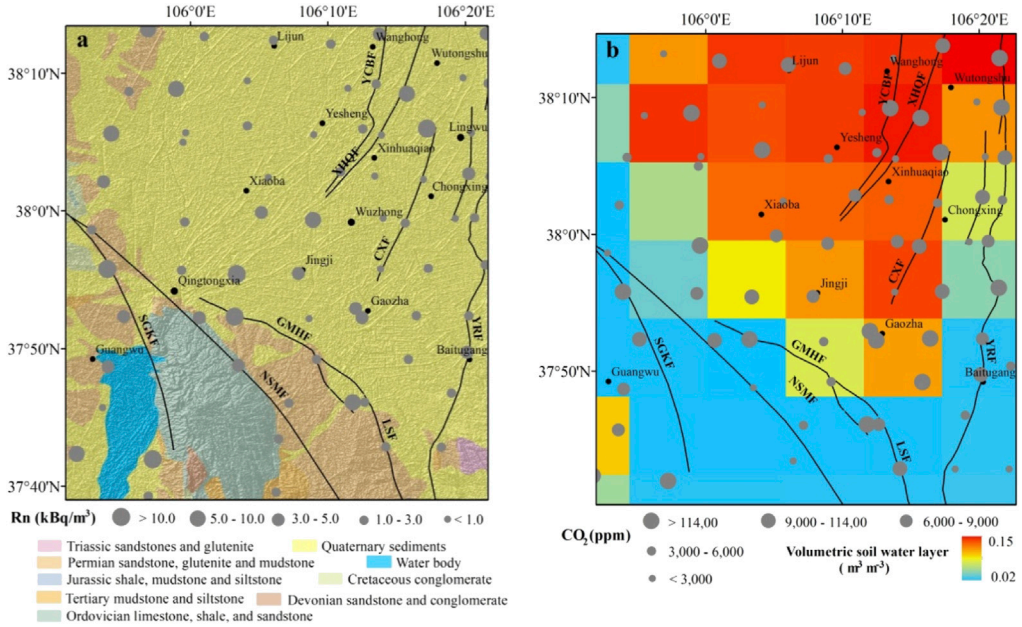

FIGURE 5
(A) Lithology and **(B)** local variance of surface latent heat flux in the Wuzhong–Lingwu area.

for CO_2 (Figure 2). The proportions of sample sites exceeding the Rn and CO_2 thresholds were 15.7% and 23.7%, respectively.

The spatial distributions of Rn and CO_2 concentrations interpolated by the IDW method were closer to measured values (i.e., smaller MAE and RMSE) than those from the OK method (Table 3). Accordingly, the spatial distributions derived using the IDW method were used for analysis. High-Rn anomalies were mainly distributed in two areas (Figure 3A): 1) western Lingwu, where the maximum value exceeded 20 kBq/m^3; and 2) southern and eastern Qingtongxia. Low-Rn areas (Rn < 0.9 kBq/m^3) were sporadically distributed to the west and south of Lingwu.

10.3389/feart.2023.1100039

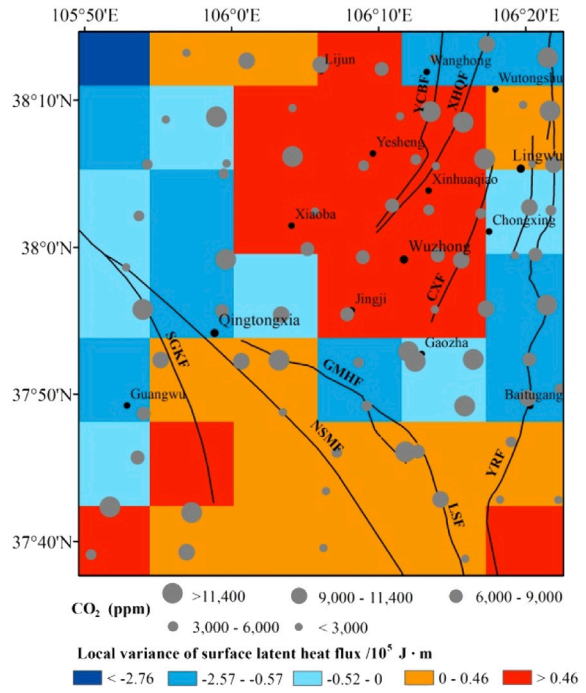

FIGURE 6
Relationship between the spatial distribution of surface latent heat flux (SLHF) and CO_2 in the Wuzhong–Lingwu area.

High-CO_2 anomalies were similar to those of Rn in eastern Qingtongxia and west of Lingwu, with the maximum value reaching 3.0% (Figure 3B). However, large areas with elevated CO_2 were also identified to the south of Gaozha, where the maximum value reached >2.3%.

A comparison of the soil gas results of the six profiles is shown in Table 4. The background value of Rn concentration in the HC, GLC, and SC profiles is slightly larger than in other YRF profiles, while the RAI is largest in the BTG and GJJT profiles. Both the background value of CO_2 concentration and the RAI on the YRF_S and YRF_M profiles are greater than the value of YRF_N.

Rn and CO_2 variation

Trace gases from Earth's subsurface can migrate to the surface together with other carrier gases; CO_2 is one of the main carrier gases for Rn (Toutain & Baubron., 1999; Yang et al., 2003; Fu et al., 2016). Gases from meteorological sources are primarily influenced by surface processes, such as air dilution and soil respiration (Sun et al., 2021); deep-seated gases are related to crustal and mantle degassing along fault zones (Sciarra et al., 2020). Figure 4 shows the variation in Rn concentration with CO_2 concentration; meteorological sources are represented by part A (low Rn and CO_2), and deep crustal and mantle gases are represented by part D (high Rn and CO_2). The Rn and CO_2 concentrations are not coupled in parts C and B. In part C, CO_2 concentrations do not increase with increasing Rn; in part B, high CO_2 (>1.0%) is found together with moderate Rn (2.0–10.0 kBq/m^3). Parts C and B can be considered shallow sources of soil and rocks. The data show that the origins of soil gas in the Wuzhong–Lingwu area are complex, with Rn and CO_2 generally derived from different sources.

Influence of surface overburden layer on soil gas Rn and CO_2

The rock type, soil type, and hydrothermal conditions of overlying strata play an important role in the distribution of soil gas concentrations, especially in areas affected by human activity. The highest Rn contents are in granite and acidic volcanic units, followed by shale, limestone, sandstone, and mafic dikes (Baixeras et al., 2001; El-Arabi et al., 2006). In the study area, the distribution of high-Rn anomalies is strongly related to Permian sandstones and mudstones in a piedmont setting (Figure 5A). Most high-CO_2 anomalies (8 of 12) are concentrated in the transition area between the mountains and basin, which is also a transition zone for soil moisture. Local variation in the July average of SLHF (Figure 6A) reveals a dramatic negative anomaly in the transition zone between the mountains and basin.

Gas concentrations are influenced by SWVL. In a certain range, SWVL will increase the thickness of an impermeable layer that will hinder the exchange of soil gas with the atmosphere and increase the soil gas concentration. However, if SWVL is excessive, soil gas will dissolve or be displaced, reducing the concentration of soil gas (Hinkle, 1994). The study area is an arid/semi-arid environment. In the mountains, bedrock is largely exposed, and vegetation cover is low. As such, the SWVL content is extremely low, and water–heat exchange is weak. In contrast, the thick (~1400 m) Quaternary sediments in the Yinchuan Basin are formed of silty clay and silt; In addition, with flat terrain, the Yinchuan basin is an important area of Yellow River irrigation planted with vegetables, corn and rice; as such, plains have higher soil moisture and a stronger water and heat exchange system. There is a negative correlation between SWVL and concentration of Rn and CO_2 in the Yinchuan Basin. However, there is a positive correlation between SWVL, and Rn and CO_2 concentrations in the mountainous areas around the basin. Accordingly, the long-term process of Yellow River irrigation in the basin has diluted the background value of Rn parent isotopes, resulting in lower Rn concentrations. Moreover, the soil in irrigated areas has a relatively high moisture content, which leads to clay leaching and a sticky soil texture (Yu et al., 2000). The consequent reduction in pores is not conducive to gas migration, blocking the release of deeper gases and contributing to the low values of Rn and CO_2. The shallow soil layer is less affected by irrigation in the transition zone between the basin and mountains, but surface soil moisture is still higher than in the mountains. Local SLHF variation is significantly negative, indicating that the evaporation of surface water is significantly decreased in the transition zone compared with the mountains. In addition, the transition zone is characterized by loosely accumulated alluvial deposits, loose soil, and low shrubs with developed roots. Humus accumulation, rich organic matter, and strong soil microorganism activity have resulted in high CO_2 emissions.

In summary, Rn anomalies in southern Qingtongxia and CO_2 anomalies in the transition area between the basin and mountains are related to underlying rocks and/or shallow soils but not seismic or tectonic activity. In contrast, environmental factors do not contribute to the high-Rn and CO_2 anomalies observed west of Lingwu.

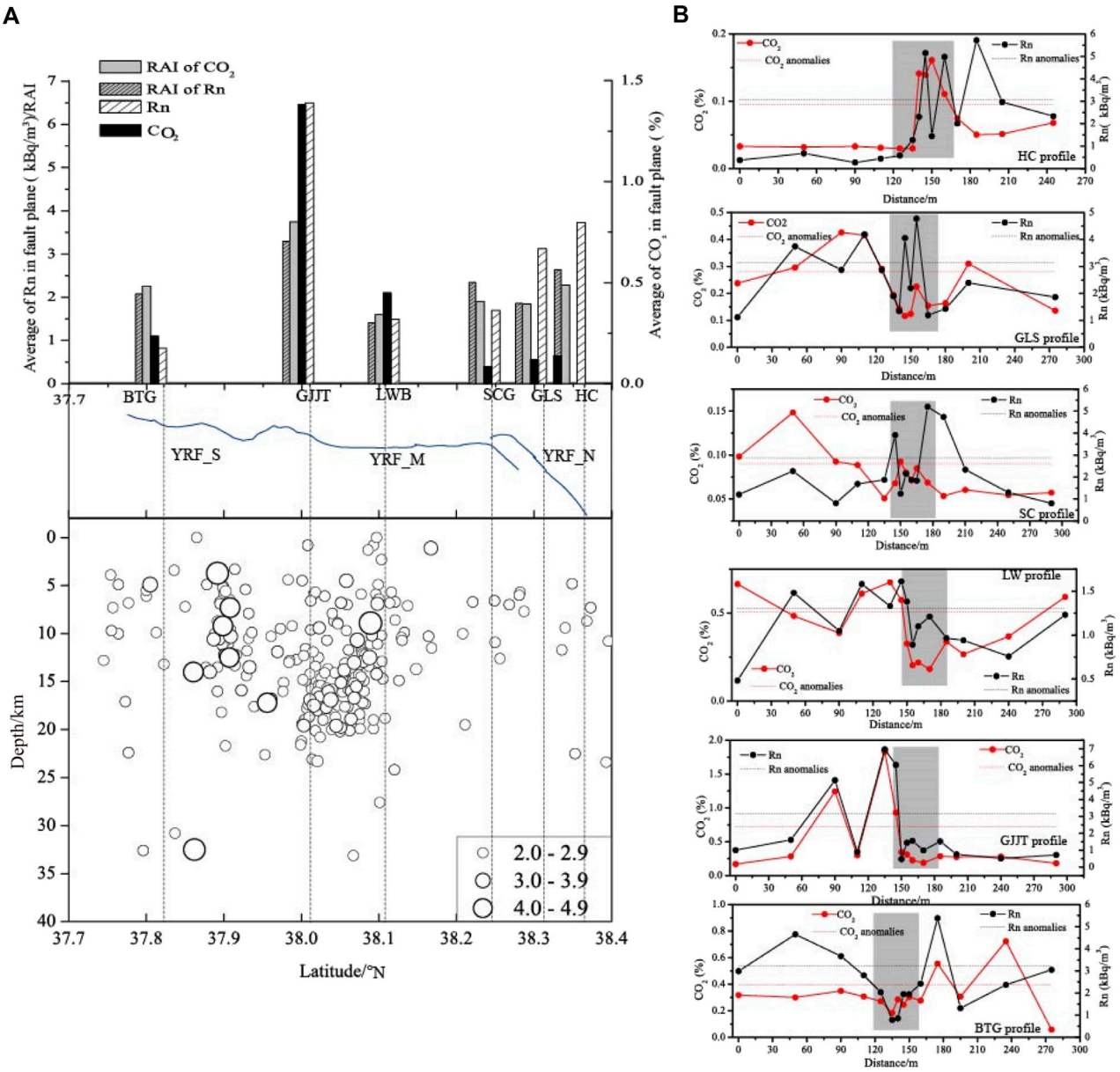

FIGURE 7
Variations in seismic activity and gas concentration along different segments of the Yellow River Fault (gray shading indicates the fault's location, The northern, middle, and southern segments of Yellow River Fault are designated as YRF_N, YRF_M, and YRF_S, respectively).

Soil gas geochemistry in different segments of Yellow River fault

As a deep-cut normal fault on the eastern border of the Yinchuan Basin, the Yellow River Fault controls the seismic activity in Wuzhong-Lingwu (Chai et al., 2001; Fang et al., 2009). According to the soil gas results across faults (Figure 7B), in the HC and GLS profiles of YRF_N, the concentration of Rn and CO_2 has a significant single peak along the fault plane, and the gas concentration differs significantly between the two sides of the fault, reflecting differences in the degree of fragmentation on each side. Moreover, these two profiles exhibit similar concentrations of Rn and CO_2 at their fault planes, being 3.73 kBq/m^3, 0.14% in the HC profile, and 3.25 kBq/m^3, 0.12% in the GLS profile, respectively. There is a significant reduction in the gas concentration in the SC section on the fault plane, and the Rn and CO_2 concentrations are only 1.70 kBq/m^3 and 0.09%. Similarly, the gas concentration on the fault plane of the LWB in YRF_M decreased sharply as well. As in the GJJT profile, the concentration of gas at the fault plane is relatively high, with Rn of 6.50 kBq/m^3 and CO_2 content of 1.38%. The gas concentrations are significantly different between the two walls, with the hanging wall gas concentration being higher and forming two peaks. As seen in the BTG profile of YRF_S, the gas concentration at the fault plane is the lowest, Rn is only 0.8 kBq/m^3, and CO_2 is only 0.24%, which is consistent with the gas emission mode of the normal fault (Annunziatellis et al., 2008), that is, a highly fragmented fault plane results in rapid gas outflow and is susceptible to air dilution and contamination with deep gas, resulting in low measured values. Additionally, most profiles of YRF exhibit the

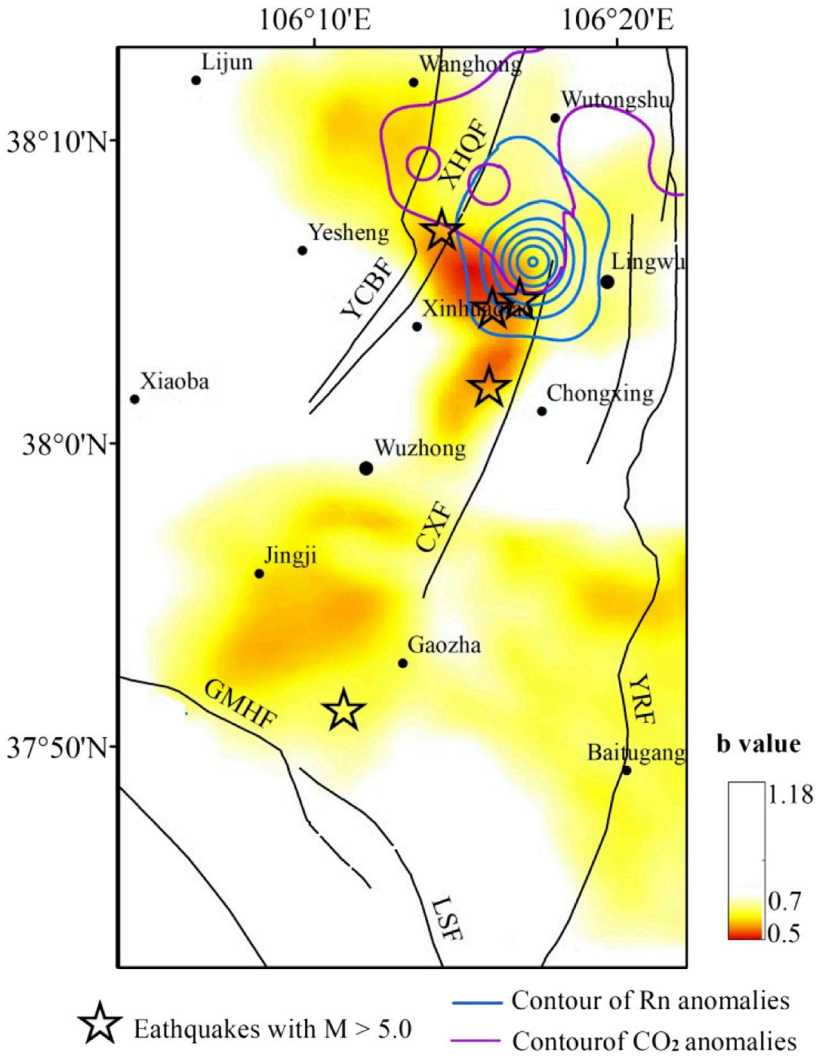

FIGURE 8
Spatial distributions of b-value and anomalies of gas in the Wuzhong–Lingwu area.

characteristics of multi-peak gas emission, which is a characteristic of strike-slip faults (Sun et al., 2017). Therefore, both strike-slip and certain normal fault characteristics have been found in YRF.

Depending on the activity of faults, underground structures, gas sources, geology and human activity within each profile, the concentration of gas released varies (Seminsky & Bobrov, 2009). Considering the distance between the sampling points and the fault plane varied, the degree of fragmentation of the underground rock and the permeability of the formation is also different. This results in variations of the soil gas concentration in the profile. CO_2 and Rn are consistently measured in most points, confirming that CO_2 is one of Rn's carrier gases.

The fault activity in the YRF_N is weak (Lei et al., 2014), and the magnitude of seismic activity in this area is small, primarily magnitude 2, with a shallow depth and low soil gas concentration and weak RAI of Rn and CO_2 were detected (Figure 7A). In the HC to SC profile, Cretaceous sandstone and glutenite are widely distributed and mixed with mudstone, contributing to the high value of Rn. It has been found that the fault in YRF_M is exposed to the surface (Chai et al., 2001), the seismic activity is relatively active, the magnitude and frequency of small earthquakes have both increased significantly, and the focal depth is deeper than what is found in the northern section, with most earthquakes occurring in the range of 5–20 km. Rn and CO_2 concentrations and RAIs were also highest in YRF. Even though the frequency of seismic activity in YRF_S is lower than in YRF_M, the intensity of seismic activity is slightly higher, and there have been numerous earthquakes above magnitude 4. Consequently, with the low concentration of gases at the fault plane, the RAI of Rn and CO_2 is not low. Frequent small earthquake increase underground rock cracks, which can result in gas emissions. At the same time, the deeper the focal depth, the more deep fluids are easier to migrate to the surface during seismic activity, thereby increasing the concentration of gas on the surface. Accordingly, the difference in seismic activity also accounts for the differences in gas concentration and RAI between segments of the YRF.

Gas migration and seismic hazard

Soil gases migrate easily from depth to the surface, making them valuable precursors of crustal transients (Bernard, 2001). The soil gas

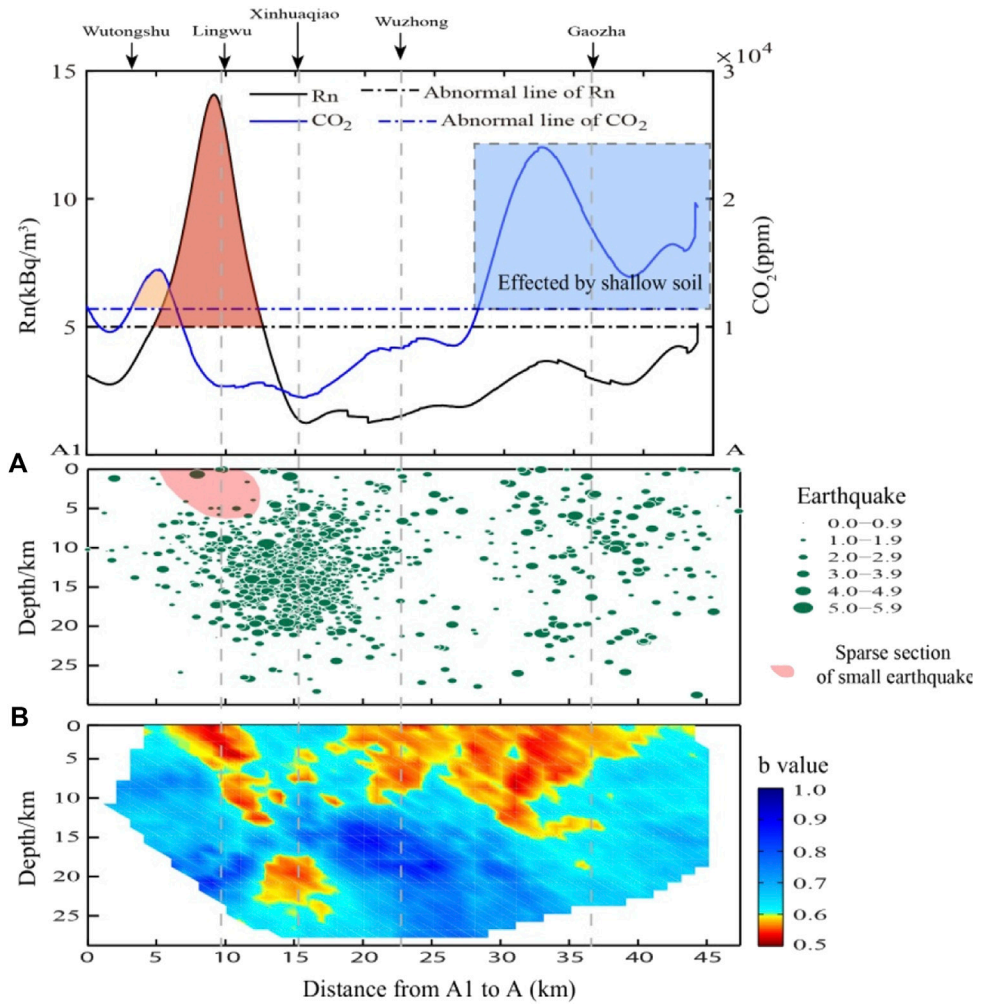

FIGURE 9
Depth profiles of **(A)** gas concentration, **(B)** earthquake scale, and **(C)** b-value in the Wuzhong–Lingwu area. The light pink shadow and dark red shadow represent the anomalies of CO2 and Rn above the threshold.

concentration is directly or indirectly related to subsurface porosity and overburden properties. Moreover, as soil gas concentrations can be related to seismic activity and fault characteristics, they offer insight into crustal stresses and strains (Pizzino et al., 2004; Chen et al., 2022). High soil gas concentrations occur in fault zones with high strain and increased seismicity (Yuce et al., 2017; Sun et al., 2021; Lombardi and Voltattorni., 2020). An inverse relation between seismic b-value and stress can usually be interpreted as a measure of the current stress level of an active fault zone (Wyss et al., 2000; Wiemer, 2001). By finding the position of the asperity structure based on lower b-values, the stress state of different sections of an active fault zone in a specific area can be determined, and the potential risk of strong earthquakes can be assessed (Yi et al., 2004).

We calculated b-values using seismic data collected by the Ningxia Network for the period from 1970 to 2020 (Zeng et al., 2021). Two areas with low b-value anomalies (<0.7) were identified, west of Lingwu and south of Wuzhong (Figure 8), suggesting high-stress levels and higher moderate earthquake risk compared with other parts of the study area. CO_2 anomalies impacted by the shallow soil environment in the transition area between the basin and mountains were removed. Similarly, Rn anomalies in southern Qingtongxia, attributed to overburden lithology, were removed. The relationship between the remaining soil gas anomalies and the b-values was determined. The low b-value in the west of Lingwu was consistent with the region of high-Rn and -CO_2 anomalies. Thus, soil gas emission in the west of Lingwu was considered the contribution to a high-stress state. Similar findings have been found in the different segments of the North-South seismic zone. The distributions of the high soil-gas concentrations in the Xianshuihe-Xiaojiang fault system (XXFS) coincide with the highest stress and maximum strain rates (Sun et al., 2021), indicating that the fault activity enhanced permeability and increased the emission rates of the gases. The relationship between radon concentration and fault activity was investigated on the northern edge of the west Qinling fault, higher radon was detected in a seismically active zone (Li et al., 2016). Furthermore, it has also been observed that the anomalous area of high gas coincides with the area of low b value and strong seismic activity in the generalized Haiyuan fault zone, which is closer to the Lingwu area (Zhou et al., 2016). Owing to the uneven distribution of fluid in crustal fractures and fault zone, variation of stress associated

with earthquakes will cause pore pressure, fluid-rock interaction and fluid migration, leading to changes in the geochemical characteristics of fluid (Lombardi & Voltattorni, 2020). Moreover, considering that the thickness of the crust increases suddenly and high-velocity bodies are widely distributed in this part of the study area (Zeng et al., 2017; Xu et al., 2018), west of Lingwu was identified as a region at risk from strong earthquakes. In fact, three earthquakes of M > 5 have occurred in the west of Lingwu since 1970. Therefore, soil gas Rn and CO_2 anomalies are important indicators for assessing the risk of moderate or strong earthquakes in the west of Lingwu.

The relationship between the b-value of the NNE profile (Figure 9) and the soil gas concentrations were determined. In the profile, western Lingwu is characterized by high-Rn and -CO_2 anomalies and low b-values. The focal depth profile also shows a sparse segment of small earthquakes and low b-values simultaneously distributed at ~5 km depth, confirming the greater risk of moderate earthquakes and that future earthquakes in this region will likely be shallow and destructive. Therefore, the relationship between low b-value and subsurface fluid anomalies also suggests that variation in the crustal state is closely related to the local fluid activity. In addition, small-magnitude seismic activity frequently occurred at a depth of 10–20 km west of Lingwu. Rock fissures opened by seismic activity in the upper crust facilitate deep gas migration, resulting in elevated Rn and CO_2 emissions (Ghosh et al., 2009; Lombardi & Voltattorni, 2010; Zhou et al., 2010).

In the south of Gaozha, low b-values are associated with frequent small earthquakes; However, the lack of credible Rn or CO_2 anomalies associated with seismic activity or high stress further indicates that the seismic risk in this area cannot currently be assessed by geochemical methods.

The frequency of seismic activity has been significantly lower than that in the west of Lingwu since 1970. Studies of low gas anomalies in some active fault zones indicated that the high locking degree of the fault constrains the migration of soil gas, whereas the creeping fault with a low locking degree is more favorable for the discharge of gas from deeper layers up toward the surface (Yang et al., 2018; Zhou et al., 2020; Yang et al., 2021). Although gas concentrations are low in the southern segment of the YRF, according to the slip rate inversed by InSAR, there is ~6.8 km locking in the southern segment of the YRF (Zhang et al., 2020), which the risk of strong earthquakes has increased. Therefore, more gas samples should be collected, and isotope analysis is needed to determine the source of the CO_2. Other deformation observations, such as leveling, Global Navigation Satellite System (GNSS), and interferometric synthetic aperture radar (InSAR), should be employed to monitor seismicity in this region.

Conclusion

This study aimed to investigate the spatial distribution and influencing factors of Rn and CO_2 in the Wuzhong–Lingwu area based on field measurements of 76 measurement points, spatial interpolation and observed results of six crossing-fault profiles along the Yellow River Fault zone (YRF). The following conclusions can be drawn.

1) Observed results of the soil gas Rn and CO_2 in different segments of YRF illustrated that YRF has features of both strike-slip and certain normal fault characteristics. Frequent seismic activity and deeper focal depth could also account for the higher gas concentration and strong RAI in the YRF.
2) The spatial distributions of Rn and CO_2 are distinct. High-Rn values are found in east and south Qingtongxia and are associated with overburden lithology. CO_2 anomalies in the transition area between the basin and mountains are related to the shallow soil environment.
3) Under the influence of irrigation by Yellow River diversion, the soil porosity was reduced, and the parent isotopes of Rn isotopes were diluted. Therefore, low values of Rn and CO_2 were widely distributed in areas with high soil moisture in the basin.
4) After removing Rn and CO_2 anomalies related to shallow soil and rocks, higher gas anomalies are consistent with low b-values in the west of Lingwu. By combining similar studies in the north-south seismic belts, it is believed that high stress and strong seismic activity increased the permeability of rocks and boosted gas emissions. In addition, a crustal thickness variation belt, the distribution of high-velocity bodies, and frequent seismic activity in west of the Lingwu area further reveal a higher seismic hazard.

Data availability statement

The original contributions presented in the study are included in the article/supplementary material, further inquiries can be directed to the corresponding author.

Author contributions

XinL contributed to the sampling, methodology, data analysis and writing. XiaL is the corresponding authors and for the language improvement and methodology. XZ contributed to the calculation of b value and data analysis of seismic activity. Other authors contributed to the sampling.

Funding

This work was supported by the National Natural Science Foundation of China [42071230], Ningxia Natural Science Foundation [2022A1335, 2020AAC03280, 2022AAC03696], Earthquake Science and Technology Spark Plan Project of China Earthquake Administration (XH20064), the Key Research and Development Program of the Ningxia Autonomous Region [2018BEG003004 and 2018BFG02011] and the innovative teams of the Earthquake Agency of Ningxia Hui Autonomous Region [CX 2019–4 9)].

Acknowledgments

The authors thank Du Jianguo for discussion of soil gas origins.

Conflict of interest

The authors declare that the research was conducted in the absence of any commercial or financial relationships that could be construed as a potential conflict of interest.

Publisher's note

References

Al-Hilal, M., and Abdul-Wahed, M. K. (2007). Tectonic and geologic influences on soil gas radon emission along the Western extension of Damascus fault, Syria. *Environ. Earth Sci.* 75 (23), 1–11. doi:10.1007/s12665-016-6292-z

Ando, T., and Ueyama, M. (2017). Surface energy exchange in a dense urban built-up area based on two-year eddy covariance measurements in Sakai, Japan. *Jpn. Urban Clim.* 19, 155–169. doi:10.1016/j.uclim.2017.01.005

Annunziatellis, A., Beaubien, S. E., Bigi, S., Ciotoli, G., Coltella, M., and Lombardi, S. (2008). Gas migration along fault systems and through the vadose zone in the Latera caldera(central Italy): Implications for CO_2 geological storage. *Int. J. Greenh.Gas Con* 2 (3), 353–372. doi:10.1016/j.ijggc.2008.02.003

Baixeras, C., Erlandsson, B., Font, L., and Jonsson, G. (2001). Radon emanation from soil samples. *Radiat. Meas.* 34, 441–443. doi:10.1016/S1350-4487(01)00203-7

Baubron, J. C., Rigo, A., and Toutain, J. P. (2002). Soil gas profiles as a tool to characterise active tectonic areas: The jaut pass example (pyrenees, France). *Earth Planet. Sci. Lett.* 196 (1–2), 69–81. doi:10.1016/s0012-821x(01)00596-9

Beaubien, S. E., Ciotoli, G., and Lombardi, S. (2003). Carbon dioxide and radon gas hazard in the Alban Hills area (central Italy). *J. Volcanol. Geotherm. Res.* 123, 63–80. doi:10.1016/s0377-0273(03)00028-3

Bernard, P. (2001). From the search of 'precursors' to the research on 'crustal transients. *Tectonophysics* 338, 225–232. doi:10.1016/s0040-1951(01)00078-6

Chai, C. Z., Liao, Y. H., Zhang, W. X., Xu, W., Shen, X., and Tian, Q. (2001). Late quaternary paleoearthquakes and their rupture features along the Lingwu fault. *Seismol. Geol.* 23 (1), 15–23. (in Chinese). doi:10.3969/j.issn.0253-4967.2001.01.002

Chen, Z., Li, y., Liu, Z. F., He, H. Y., Martinellib, G., Lu, C., et al. (2022). Geochemical and geophysical effects of tectonic activity in faulted areas of the North China Craton. *Chem. Geol.* 609, 1–11. doi:10.1016/j.chemgeo.2022.121048

Ciotoli, G., Lombardi, S., and Annunziatellis, A. (2007). Geostatistical analysis of soil gas data in a high seismic intermontane basin: Fucino Plain, central Italy. *J. Geophys. Res. Solid Earth* 112, B05407–B05423. doi:10.1029/2005jb004044

Cui, Y., Du, J., Zhang, D., and Sun, Y. (2013). Anomalies of total column CO and O3 associated with great earthquakes in recent years. *Nat. Hazard. Earth Syst. Sci.* 13, 1–7. doi:10.5194/nhess-13-2513-2013

Dogan, T., Mori, T., Tsunomori, F., and Notsu, K. (2007). Soil H_2 and CO_2 surveys at several active faults in Japan. *Pure Appl. Geophys.* 164, 2449–2463. doi:10.1007/s00024-007-0277-5

El-Arabi, A., Abbady, A., Ahmed, N., Michle, R., El-Kamel, A. H., and Abbady, A. G. E. (2006). Assessment of radon-222 concentrations and exhalation rates of rocks and building materials. *Indian. J.Pure Appl. Phys.* 44 (4), 287–291. doi:10.1016/j.apradiso.2004.10.010

Fang, S. M., Zhao, C. B., Chai, Z. Z., Liu, B. J., Feng, S. Y., Liu, M. J., et al. (2009). Seismic evidence of crustal structures in the Yinchuan faulted basin. *Chin. J. Geophys* 52 (7), 1768–1775. doi:10.3969/j.issn.0001-5733.2009.07.010

Fu, C. C., Yang, T. F., Walia, V., and Chen, C. H. (2005). Reconnaissance of soil gas composition over the buried fault and fracture zone in southern Taiwan. *Geochem. J.* 39, 427–439. doi:10.2343/geochemj.39.427

Fu, C. C., Yang, T. F., Du, J., Walia, V., Chen, Y. G., Liu, T. K., et al. (2008). Variations of helium and radon concentrations in soil gases from an active fault zone in southern Taiwan. *Radiat. Meas.* 43, 348–352. doi:10.1016/j.radmeas.2008.03.035

Fu, C. C., Yang, T. F., Tsai, M. C., Lee, L. C., Liu, T. K., Walia, V., et al. (2016). Exploring the relationship between soil degassing and seismic activity by continuous radon monitoring in the Longitudinal Valley of eastern Taiwan. *Chem. Geol.* 469, 1–48. doi:10.1016/j.chemgeo.2016.12.042

Ghosh, D., Deb, A., and Sengupta, R. (2009). Anomalous radon emission as precursor of earthquake. *J. Appl. Geophys.* 69 (2), 67–81. doi:10.1016/j.jappgeo.2009.06.001

Giammanco, S., Gurrieri, S., and Valenza, M. (1998). Anomalous soil CO_2 degassing in relation to faults and eruptive fissures on Mount Etna (Sicily, Italy). *Bull. Volcanol.* 60, 252–259. doi:10.1007/s004450050231

Guerra, M., and Lombardi, S. (2001). Soil-gas method for tracing neotectonic faults in clay basins the Pisticci field (Southern Italy). *Tectonophysics* 339, 511–522. doi:10.1016/s0040-1951(01)00072-5

Han, X. K., Li, Y., Du, J. G., Zhou, X., Xie, C., and Zhang, W. (2014). Rn and CO_2 geochemistry of soil gas across the active fault zones in the capital area of China. *Nat. Hazard. Earth Syst. Sci.* 14, 2803–2815. doi:10.5194/nhess-14-2803-2014

Hinkle, M. E. (1994). Environmental conditions affecting concentrations of He, CO_2, O_2 and N_2 in soil-gases. *Appl. Geochem.* 9, 53–63. doi:10.1016/0883-2927(94)90052-3

Hong, W. L., Yang, T. F., Walia, V., Lin, S. J., Fu, C. C., Chen, Y. G., et al. (2010). Nitrogen as the carrier gas for helium emission along an active fault in NW Taiwan. *Appl. Geochem* 25, 593–601. doi:10.1016/j.apgeochem.2010.01.016

Irwin, W. P., and Barnes, I. (1980). Tectonic relations of carbon dioxide discharges and earthquakes. *Res. Solid Earth* 85, 3115. doi:10.1029/jb085ib06p03115

Jiao, Z. H., Zhao, J., and Shan, X. J. (2018). Pre-seismic anomalies from optical satellite observations: A review. *Nat. Hazard. Earth Syst. Sci.* 18, 1013–1036. doi:10.5194/nhess-18-1013-2018

Khilyuk, L. F., Chilingar, G. V., Robertson, J. O., Jr, and Endres, B. (2000). *Gas migration: Events preceding earthquakes*. Houston, Texas: Gulf Publishing Company.

King, C. Y., King, B. S., Evans, W. C., and Zhang, W. (1996). Spatial radon anomalies on active faults in California. *Appl. Geochem.* 11, 497–510. doi:10.1016/0883-2927(96)00003-0

Kumar, A., Singh, S., Mahajan, S., Bajwa, B. S., Kalia, R., and Dhar, S. (2009). Earthquake precursory studies in Kangra valley of North West Himalayas, India, with special emphasis on radon emission. *Appl. Radiat. Isot.* 67 (10), 1904–1911. doi:10.1016/j.apradiso.2009.05.016

Lei, Q. Y., Chai, C. Z., Zheng, W. J., Peng, D. U., Xie, X. F., Wang, Y., et al. (2014). Activity and slip rate of the northern section of Yellow River fault revealed by drilling. *Seismol. Geol.* 36 (2), 464–477. doi:10.3969/j.issn.0253-4967.2014.02.015

Li, Y., Du, J. G., Wang, F. K., Zhou, X., Pan, X., and Wei, R. (2009). Geochemical characteristics of soil gas in the Yanhuai basin, northern China. *Earthq. Sci.* 22, 93–100. doi:10.1007/s11589-009-0093-3

Li, Y., Du, J. G., Wang, X., Zhou, X., Xie, C., and Cui, Y. (2013). Spatial variations of soil gas geochemistry in the Tangshan area of Northern China. *Terr. Atmos. Ocean. Sci.* 24 (3), 323–333. doi:10.3319/tao.2012.11.26.01(tt)

Li, C. H., Su, H. J., Zhang, H., and Zhou, H. L. (2016). Correlation between the spatial distribution of radon anomalies and fault activity in the northern margin of West Qinling Fault Zone, Central China. *J. Radioanal. Nucl. Chem.* 308, 679–686. doi:10.1007/s10967-015-4504-8

Liao, Y. H., Chai, C. Z., Zhang, W. X., and Xu, W. J. (2000). The active features and slip rate of Lingwu faults in late quaternary. *Earthq. Res. Chin.* 16 (2), 158–165. (in Chinese). doi:10.3969/j.issn.1001-4683.2000.02.008

Liu, Z. F., Li, Y., Chen, Z., Zhao, Z. D., Huangfu, R. L., Zhao, Y. X., et al. (2022). Environmental impacts of ^{222}Rn, Hg and CO_2 emissions from the fault zones in the Western margin of the Ordos block, China. *Environ. Geochem. Health* 08, 1–16. doi:10.1007/s10653-022-01350-5

Lombardi, S., and Voltattorni, N. (2010). Rn, He and CO2 soil gas geochemistry for the study of active and inactive faults. *Appl. Geochem.* 25 (8), 1206–1220. doi:10.1016/j.apgeochem.2010.05.006

Ma, H. Q., Ren, X. M., Jin, C. H., and Shen, J. Q. (2006). 2003~2004 seismicity analysis of the Wuzhong and Lingwu region. *J. Seismol. Res.* 29 (2), 114–117. (in Chinese). doi:10.3969/j.issn.1000-0666.2006.02.002

Neri, M., Giammanco, S., Ferrera, E., Patanè, G., and Zanon, V. (2011). Spatial distribution of soil radon as a tool to recognize active faulting on an active volcano: The example of Mt. Etna (Italy). *J. Environ. Radioact.* 102, 863–870. doi:10.1016/j.jenvrad.2011.05.002

Pizzino, L., Burrato, P., Quattrocchi, F., and Valensise, G. (2004). Geochemical signatures of large active faults: The example of the 5 February 1783, Calabrian earthquake (southern Italy). *J. Seismol.* 8, 363–380. doi:10.1023/b:jose.0000038455.56343.e7

Sciarra, A., Cantucci, B., Sapia, V., De Ritis, R., Ricci, T., Civico, R., et al. (2020). Geochemical and geoelectrical characterization of the Terre Calde di Medolla (Emilia-Romagna, northern Italy) and relations with 2012 seismic sequence. *J. Geochem. Explor.* 221, 106678. doi:10.1016/j.gexplo.2020.106678

Seminsky, K. Z., and Bobrov, A. A. (2009). Radon activity of faults (Western Baikal and southern Angara areas). *Russ. Geol. Geophys.* 50 (8), 682–692. doi:10.1016/j.rgg.2008.12.010

Sun, X. L., Yang, P. T., Xiang, Y., Si, X. Y., and Liu, D. L. (2017). Across-fault distributions of radon concentrations in soil gas for different tectonic environments. *Geosci. J.* 22, 227–239. doi:10.1007/s12303-017-0028-2

Sun, Y., Zhou, X., Yan, Y., Li, J., Fang, W., Wang, W., et al. (2021). Soil degassing from the xianshuihe–xiaojiang fault system at the eastern boundary of the chuan–dian rhombic block, southwest China. *Front. Earth Sci.* 9, 1–12. doi:10.3389/feart.2021.635178

Szabó, K. Z., Jordan, G., Horváth, Á., and Szabó, C. (2014). Mapping the geogenic radon potential: Methodology and spatialanalysis for central Hungary. *J. Environ. Radioact.* 129, 107–120. doi:10.1016/j.jenvrad.2013.12.009

Toutain, J. P., and Baubron, J. C. (1999). Gas geochemistry and seismotectonics: A review. *Tectonophysics* 304, 1–27. doi:10.1016/s0040-1951(98)00295-9

Tramutoli, V., Cuomo, V., Filizzola, C., Pergola, N., and Pietrapertosa, C. (2005). Assessing the potential of thermal infrared satellite surveys for monitoring seismically active areas: The case of Kocaeli (İzmit) earthquake, August 17, 1999. *Remote Sens. Environ.* 96 (3–4), 409–426. doi:10.1016/j.rse.2005.04.006

Tramutoli, V., Aliano, C., Corrado, R., Filizzola, C., Genzano, N., Martinello, G., et al. (2013). On the possible origin of thermal infrared radiation (TIR) anomalies in earthquake-prone areas observed using robust satellite techniques (RST). *Chem. Geol.* 339, 157–168. doi:10.1016/j.chemgeo.2012.10.042

Weinlich, F. H. (2014). Carbon dioxide controlled earthquake distribution pattern in the NW Bohemian swarm earthquake region, Western Eger Rift, Czech Republic–gas migration in the crystalline basement. *Geofluids* 14, 143–159. doi:10.1111/gfl.12058

Wiemer, S. (2001). A software package to analyze seismicity: Zmap. *Seismol. Res. Lett.* 72 (2), 373–382. doi:10.1785/gssrl.72.3.373

Wyss, M., Schorlemmer, D., and Wiemer, S. (2000). Mapping asperities by minima of local recurrence time: San Jacinto-Elsinore fault zones. *J. Geophys. Res.* 105, 7829–7844. doi:10.1029/1999jb900347

Xu, Y. C., Wang, Q., Zeng, X. W., Ma, H. Q., Xu, W. J., and Jin, T. (2018). Moho depth and Poisson's ratio distribution in the Western edge of Ordos block. *Acta Seismol. Sin.* 40 (5), 563–581. doi:10.11939/jass.20170224

Yang, T. F., Chou, C. Y., Chen, C.-H., Chyi, L. L., and Jiang, J. H. (2003). Exhalation of radon and its carrier gases in SW Taiwan. *Radiat. Meas.* 36, 425–429. doi:10.1016/s1350-4487(03)00164-1

Yang, Y., Li, Y., Guan, Z. J., Chen, Z., Zhang, L., Lv, C. J., et al. (2018). Correlations between the radon concentrations in soil gas and the activity of the Anninghe and the Zemuhe faults in Sichuan, southwestern of China. *Appl. Geochem.* 89, 23–33. doi:10.1016/j.apgeochem.2017.11.006

Yang, Y., Li, Y., Li, Y. G., Ji, L. Y., Gong, Y., Du, F., et al. (2021). Present-day activity of the Anninghe fault and Zemuhe fault,southeastern Tibetan Plateau, derived from soil gas CO_2 emissions and locking degree. *Earth. Space. Sci.* 8, 1–21. doi:10.1029/2020EA001607

Yi, G., Wen, X., Xin, H., Qiao, H.-Z., Wang, S.-W., and Gong, Y. (2004). Stress state and major earthquake risk on the southern segment f the Longmen Shan fault zone. Chin. *J. geophys.* 56, 1112–1120. doi:10.6038/cjg20130407

Yu, J. P., Wen, Y. C., Wang, Y. M., and Song, N. P. (2000). Impacts of irrigation on soil environment by lifting up water from the Yellow River in Ningxia. *Prog. Geogr.* 19 (3), 279–284. doi:10.11820/dlkxjz.2000.03.012

Yuce, G., Fu, C. C., Alessandro, W. D., Gulbay, A. H., Lai, C. W., Bellomo, S., et al. (2017). Geochemical characteristics of soil radon and carbon dioxide within the dead sea fault and karasu faultin the amik basin (hatay), Turkey. *Chem. Geol.* 469, 129–146. doi:10.1016/j.chemgeo.2017.01.003

Zeng, X. W., Feng, J. G., Long, F., and Xin, H. L. (2017). Mid-upper crustal velocity tomography of pg wave in western margin of ordos. *J. Seismol. Res.* 40 (02), 176–185. (in Chinese).

Zeng, X. W., Li, W. J., Ma, C. Z., and Cai, X. H. (2021). Strong earthquake risk in Wuzhong–Lingwu region of Ningxia based on b value. *J. Seismol. Res.* 44 (1), 41–48. (in Chinese). doi:10.3969/j.issn.1000-0666.2021.01.006

Zhang, W. T., Ji, L. Y., Zhu, L. Y., Xu, X. X., and Wang, J. S. (2020). Current crustal deformation of Yinchuan Basin based on Sentinel-1 data. *J.Geod. Geodyn.* 40 (9), 902–917. (in Chinese). doi:10.14075/j.jgg.2020.09.005

Zhou, X., Du, J., Chen, Z., Cheng, J., Tang, Y., Yang, L., et al. (2010). Geochemistry of soil gas in the seismic fault zone produced by the Wenchuan Ms 8.0 Earth quake, southwestern China. *Geochem. Trans.* 11 (5), 5–10. doi:10.1186/1467-4866-11-5

Zhou, H. L., Su, H. J., Zhang, H., and Li, C. (2017). Correlations between soil gas and seismic activity in the Generalized Haiyuan Fault Zone, north-central China. *Nat. Hazard.* 85, 763–776. doi:10.1007/s11069-016-2603-7

Zhou, H. L., Su, H. J., Zhang, L., Li, C. H., Ma, D. Z., and Bai, R. L. (2020). Geochemical characteristics of soil gas and strong SeismicHazard potential in the liupanshan Fault Zone (LPSFZ). *Geofluids* 10, 1–14. doi:10.1155/2020/4917924